Aalborg Universitet

AALBORG UNIVERSITY

DENMARK

Operation and thermal loading of three-level Neutral-Point-Clamped wind power converter under various grid faults

Ma, Ke; Blaabjerg, Frede; Liserre, Marco

Operating and Loading Conditions of Three-level Neutral-Point-Clamped Wind Power Converter under Various Grid Faults

K. Ma, M. Liserre, F. Blaabjerg

Department of Energy Technology, Aalborg University
Pontoppidanstraede 101, DK-9220 Aalborg East, Denmark
kema@et.aau.dk, mli@et.aau.dk, fbl@et.aau.dk

Abstract – **In order to fulfill the growing demands from the grid side, the full-scale power converters are becoming popular in the wind turbine system. The Low Voltage Ride Through (LVRT) requirements may not only cause the control problems but also result in overstressed components for the power converter. However the thermal loading of the wind power converter under various grid faults is still not yet clarified especially at MW power level. In this paper, the impacts by three types of grid faults to a three-level Neutral-Point-Clamped (3L-NPC) wind power converter in terms of operating and loading conditions are analytically solved and simulated. It has been found that the operating and loading of converter under LVRT strongly depend on the types/severities of grid voltage dips and also the chosen control algorithms. The thermal distribution among the three-phases of converter may be quite uneven and some devices are much more stressed than the normal operating condition.**

Index Terms – **Wind power generation, multilevel converter, LVRT, thermal loading.**

I. INTRODUCTION

As a promising and fast growing renewable energy source, the accumulated capacity of wind power generation has achieved 238 GW globally in 2011 [1]. Meanwhile, the power capacity of individual wind turbine is also increasing continuously to reduce the price per produced kWh. In 2012, 8 MW wind turbines with diameter of 164 m have already been presented to the market [2]-[4], and the newly established wind turbines are mainly located at remote area. As a result, due to more significant impacts to the grid stability and high cost for maintenance/repair, the reliability and ability to withstand grid disturbances are greatly emphasized for the modern wind turbines.

The Transmission System Operators (TSO) in different countries have issued stricter Low Voltage Ride Through (LVRT) codes for the Wind Turbine Systems (WTS), as shown in Fig. 1 [5], in which the boundaries for dipping amplitudes of grid voltage and the disturbing time are defined. Moreover, it is becoming a need that the WTS should provide some reactive power (up to 100 % current capacity) to help the grid recover during voltage dips. Fig. 2 shows an example from German grid codes in which the required reactive current against to the amplitude of grid voltage is specified [6].
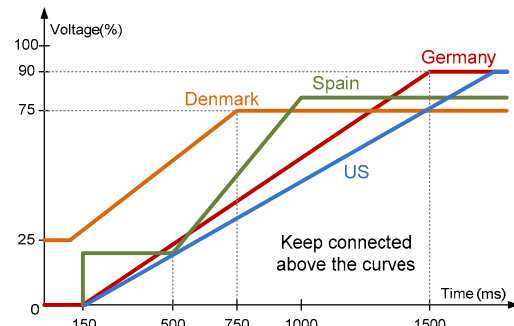

Fig. 1. Grid codes of wind turbines under low voltage ride through by different countries [5].
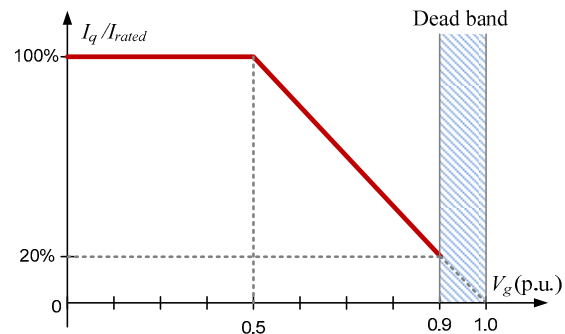
Fig. 2. Reactive current requirements vs. grid voltage V_g during low voltage ride through [6].

The stricter LVRT codes as well as the higher requirements for reliability push the solutions of WTS moving from Doubly Fed Induction Generator (DFIG) with partial-scale power converter to Asynchronous/Synchronous Generator with full-scale power converter [7]. Intensive research have been devoted to the control and PLL strategies of wind power converter under the grid faults [8]-[12], and there is also some investigations regarding the thermal loading and modulation of converter under balanced LVRT condition [13], [14]. However the operating and loading states of converter under various LVRTs (including unbalanced faults) have not been comprehensively investigated. These uncertainties could result in uneven utilization of power devices, under-estimated rating of components, and compromised reliability performances for the wind power converters [13].

Consequently, this paper will focus on the loading states of a 10 MW full-scale 3L-NPC converter under various

LVRT conditions. First, the impacts of various grid faults to the AC bus voltages and the converter operations are simulated and analytically solved. Afterwards the corresponding loss and thermal behaviors of the power semiconductor devices in the given wind power converter will be presented.

II. Voltage Dips under Various Grid Faults

When a short-circuit fault happens in the power grid system, normally the voltage dips will be detected by the grid-connected converter through the AC bus it is connected, and then the corresponding LVRT control algorithm of the Wind Turbine System (WTS) is activated, making the converter shift from the normal operation mode to the LVRT mode. However, depending on the types and locations of the short circuit, the line impedance and configuration of transformer windings, the voltage dips may vary significantly on different AC buses in the power grid [15], [16]. Therefore, it is important first to investigate how the voltage dip looks like on the bus where the WTS is connected.

A typical configuration of a WTS with the grid system is shown in Fig. 3, in which the voltage on Bus 2 is monitored by the WTS and hence determines the LVRT behavior of the wind power converter. A delta-star transformer is used to interface the WTS on Bus 2 (e.g. 3.3 kV) and the Point of Common Coupling (PCC) on Bus 1 (e.g. 20 kV). Other power sources and loads in the distribution system may be also connected to the Bus 1. It is assumed that a short-circuit fault happens somewhere with line impedance Z_F to the Bus 1 (PCC), and the line impedance from PCC to the grid with higher voltage level is Z_s.
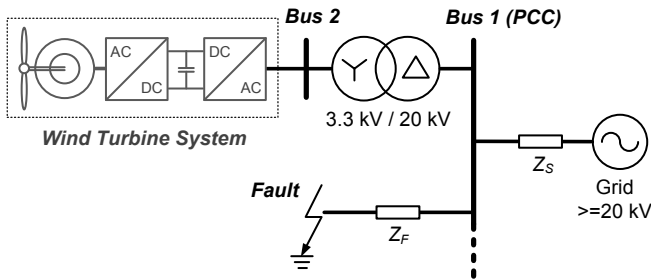

Fig. 3. Typical bus configuration for grid integration of a WTS (a shot circuit fault is indicated).

Define that the voltage dip severity on Bus N is D_N, which is related to the location of grid faults and power line impedance. Providing that the line impedances for the positive and negative sequence components are equal, the dip severity on the Point of Common Coupling (or Bus 1) D_1 can be written as [16]:

$$D_1 = \frac{Z_F}{Z_F + Z_S} \qquad (1)$$

It is obvious that D_1 ranges from 0 (if $Z_F=0$) to 1 (if $Z_S=0$), and represents the voltage dipping severities from the most severe case ($D_1=0$) to the non-dip case ($D_1=1$).

Three typical grid faults: one-phase grounded (1 phase), two-phase connected (2 phase) and three-phase grounded (3 phase) are assumed to happen respectively at the same location of the power grid. Due to the delta-star connection of the transformer, the voltage dips on Bus 1 may have different characteristics when propagated on Bus 2. The dip type, dip severity and voltage amplitude of different grid faults are summarized in Table I, in which the voltage parameters seen on Bus 1 and Bus 2 are identified respectively. The voltage dipping type A-D is defined as phasor diagrams in Fig. 4 [15], [16].

Table I. Voltage dip seen on Bus 1 and Bus 2 for various grid faults.

Fault type		One-phase	Two-phase*	Three-phase
Bus1 (PCC)	Dip type	B	C	A
	Dip value D_1**		$D_1 \angle 0°$	
	Voltage amplitude*** V_{1min} (p.u.)	D_1	$0.5\sqrt{1+(\sqrt{3}D_1)^2}$	D_1
Bus2 (WTS)	Dip type	C	D	A
	Equivalent dip value D_2	$\frac{D_1+0.5}{1.5} \angle 0°$	$D_1 \angle 0°$	$D_1 \angle 0°$
	Voltage amplitude*** V_{2min} (p.u.)	$0.5\sqrt{1+(\sqrt{3}D_2)^2}$	D_2	D_2

Notes:
* Two-phase grounded fault is not included because it seldom happens.
** No phase jump is assumed, i.e. vector D_1 has zero phase angle.
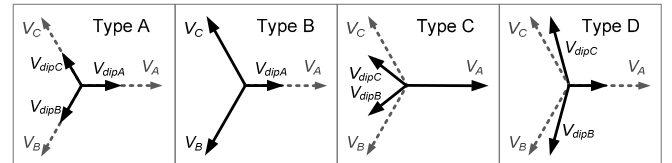*** Voltage amplitude means the lowest one among the three phases.

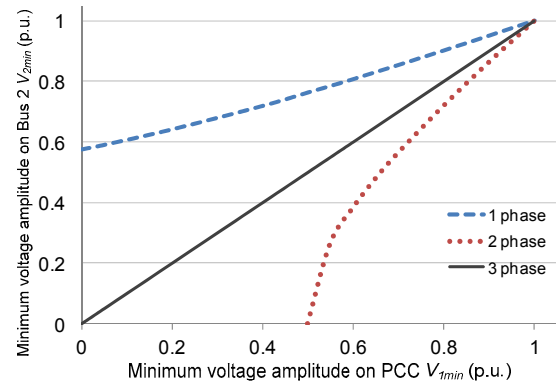Fig. 4. Phasor diagram definitions for the dip types A-D specified in Table I.

Fig. 5. Minimum voltage amplitude on Bus 2 vs. Bus 1.

The relationship between the minimum voltage amplitude among three-phases on Bus 1 V_{1min} and the minimum voltage amplitude on Bus 2 V_{2min} are plotted in Fig. 5, in which balanced (three-phase) and unbalanced (one-phase and two-phase) grid faults are indicated respectively. It is noted that because Bus 2 is directly monitored by the wind power converter, only V_{2min} will determine the amount of reactive current injected into the power grid by converter.

III. LVRT OPERATION OF GRID-CONNECTED CONVERTER UNDER VARIOUS GRID FAULTS

In order to determine the loading of the power semiconductor devices, it is important to study how the grid-converter behaves under various grid voltage dips. Depending on the AC bus voltage and active/reactive power injection methods, the current and voltage amplitudes as well as their phase displacement of the grid converter may vary considerably and create different operation scenarios.

A. Converter system under investigation

As the widely commercialized multilevel topology which is used in the high-power medium-voltage applications for industry, mining, and traction [17], the three-level neutral-point-clamped (3L-NPC) solution seems to be a promising candidate for the Multi-MW full-scale wind power converter [18]-[20], as shown in Fig. 6. This topology is chosen and basically designed for a 10 MW wind turbine as a case study in this paper [19]-[22], where the major design parameters are summarized in Table II.

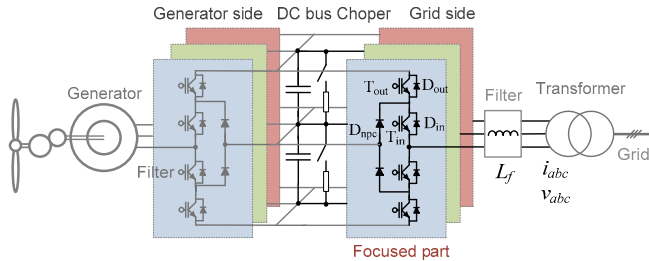Fig. 7 shows the control scheme adopted to deal with

Fig. 6. Three-level Neutral point clamped converter used in a WTS.

Table II. Parameters of three-level Neural Point Clamped inverter for case study

Rated output active power P_o	10 MW
DC bus voltage V_{dc}	5.6 kV DC
*Rated primary side voltage V_p	3.3 kV rms
Rated line-to-line grid voltage V_g	20 kV rms
Rated load current I_{load}	1.75 kA rms
Carrier frequency f_c	750 Hz
Filter inductance L_f	1.1 mH (0.25 p.u.)

* Line-to-line voltage in the primary windings of transformer.
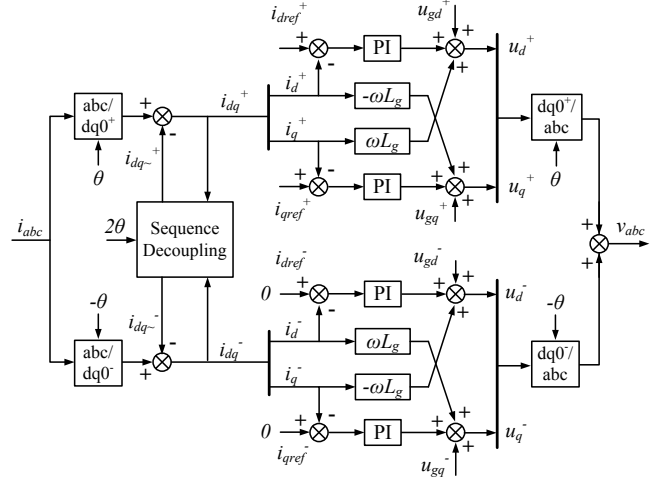

Fig. 7. Current control scheme of the grid-side converter.
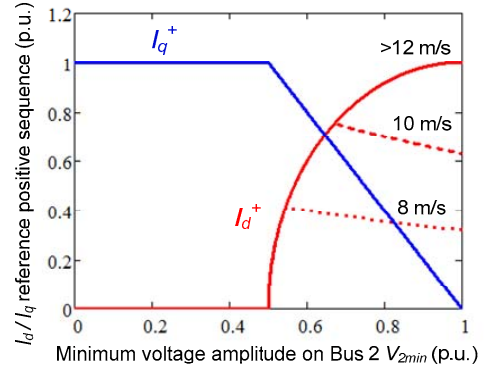
Fig. 8. Current references in positive sequence vs. minimum voltage amplitude on Bus 2.

unbalanced grid faults: both positive and negative sequences voltages/currents are detected and controlled. A sequence decoupling algorithm is used to remove the 100 Hz oscillation components in each of the sequence domain [11], [12]. It is worth to mention that the currents injection strategy under various grid faults is still an issue for discussion, in this paper it is assumed that the active and reactive current generated by the grid-converter only contains positive sequence component, and this can be achieved by setting the references for negative sequence currents to zero when using the control method shown in Fig. 7.

The references for positive sequence current as a function of the minimum voltage amplitude on Bus 2 V_{2min} are specified in Fig. 8, where the current I_q^+ is set according to the German grid code reported in Fig. 2, and the current I_d^+ is referred to the generated active power by wind turbines. It is assumed that the converter is set to provide as much active power as possible during the grid faults, and the pitch control does not have enough time to activate [8], [9]. This is the worst testing condition for the wind power converter.

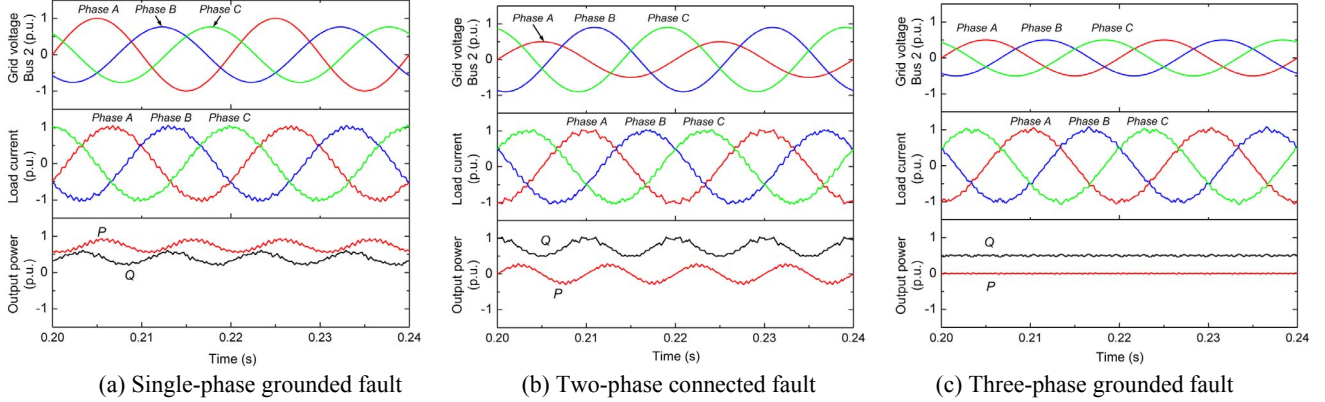(a) Single-phase grounded fault (b) Two-phase connected fault (c) Three-phase grounded fault

Fig. 9. Outputs of 3L-NPC converter under various grid faults. (D_1=0.5 p.u., v_w=12 m/s, German grid codes)

B. An example when D_1=0.5 p.u.

As an example to understand the converter status under LVRT, Fig. 9 gives the converter outputs under three types of grid faults with the same dip severity D_1=0.5 p.u.. The voltage on Bus 2, load current and the instantaneous active/reactive power are shown respectively. The parameters for the bus voltage under each given fault conditions are summarized in Table III, and the wind speed is set at 12 m/s when the wind turbine generates the rated 10 MW active power.

As it can be seen from Fig. 9, the voltages on Bus 2 under each given grid fault condition are consistent with the fault definition in Fig. 4, and the currents are symmetrical among the three phases, which means only positive sequence currents are injected. Due to the existence of negative

Table III. Voltage dips for example (D_1=0.5 p.u.).

	Fault type	1 phase	2 phase	3 phase
Bus1 (PCC)	Dip type	B	C	A
	Dip value D_1		0.5	
Bus2 (WTS)	Dip type	C	D	A
	Equivalent dip value D_2	0.67	0.5	0.5
	Voltage amplitude* V_{2min} (p.u.)	0.76	0.5	0.5
	Positive sequence $V_2{}^+$ (p.u.)	0.833	0.75	0.5
	Negative sequence $V_2{}^-$ (p.u.)	0.167	-0.15	0

* Voltage amplitude means the lowest one among the three phases.

Table IV. Positive and negative sequence voltage on Bus 2 for different fault types.

	Fault type	1 phase	2 phase	3 phase
Bus2	Dip type	C	D	A
	Positive sequence $V_2{}^+$ (p.u.)	$0.5 \cdot (1+D_2)$	$0.5 \cdot (1+D_2)$	D_2
	Negative sequence $V_2{}^-$ (p.u.)	$0.5 \cdot (1-D_2)$	$-0.5 \cdot (1-D_2)$	0

sequence voltage, there is a 100 Hz oscillation in the delivered active and reactive power under one-phase and two-phase unbalanced grid faults. This 100 Hz power oscillation is assumed to be absorbed by the DC bus chopper during LVRT operation.

C. Operation profiles with various dip severity and wind speeds.

After the bus voltage dips and corresponding converter behaviors are specified, it is possible to calculate the operating profiles of converter under various grid faults. In this paper the profiles for the delivered active/reactive power, phase displacement between current and voltage, and the modulation index are going to be investigated because they are closely related to the loading of switching devices.

If the grid voltage is aligned with the d axis in the rotating coordinate, and the negative sequence currents are controlled to be zero, the active power P and reactive power Q delivered into the power grid are governed by:

$$P = \frac{3}{2}V_d^+ \cdot I_d^+ = \frac{3}{2}V_2^+ \cdot I_d^+$$
$$Q = \frac{3}{2}V_d^+ \cdot I_q^+ = \frac{3}{2}V_2^+ \cdot I_q^+ \tag{1}$$

where the d axis positive sequence voltage V_d^+ is equal to the positive sequence voltage on bus 2 V_2^+, which is given in Table IV for various grid fault conditions.

Then the positive sequence currents I_d^+ and I_q^+ generated by the converter can be calculated as:

$$I_q^+ = \sqrt{2}I_{rated} \cdot R_{codes}$$
$$I_d^+ = \min\left[\sqrt{2}I_{rated}\sqrt{1-R_{codes}^2} \ , \ \frac{2P_G(v_w)}{3V_d^+}\right] \tag{2}$$

where I_{rated} is the rated load current, $P_G(v_w)$ is the generated active power by the wind turbines, it is related to the wind speeds and the functions can be found in [23]. R_{codes} is the reactive current ratio required by the German grid codes [6], it can be analytically represented as:

$$R_{codes} = \min\left[2 \cdot (1 - V_{2\min}) , 1\right] \quad (3)$$

Fig. 10 gives the operation profile for the average active and reactive power delivered by the wind power converter at different dip severity on PCC (D_1). The situations with one-phase, two-phase and three-phase grid faults are shown in Fig. 10 (a), Fig. 10 (b) and Fig. 10 (c) respectively. It can be seen that the delivered active/reactive powers are significantly different under the three types of grid faults, especially when D_1 is below 0.5 p.u.

For the phase angle displacement between load current and bus voltage in each phase θ_A, θ_B and θ_C, they can be calculated as:

$$\theta_A = -\arctan(\frac{I_q^+}{I_d^+})$$
$$\theta_B = -\left[\theta_A - (\frac{\pi}{3} - \arctan(\sqrt{3} \cdot D_2))\right] \quad (4)$$
$$\theta_C = -\left[\theta_A + (\frac{\pi}{3} - \arctan(\sqrt{3} \cdot D_2))\right]$$

Fig. 11 shows the phase displacement with relation to the dip severity on PCC, where different wind speed conditions are indicated. Obviously, the phase angles in the three types of grid faults all increase with the decrease of D_1. The maximum phase angle difference among the 3 phases achieve 60° for both of the unbalanced grid fault conditions when $D_1=0$ p.u.. It can also be observed that the wind speeds have strong impacts to the phase angle of the power converter under various LVRT operations.

The modulation index for phase X (A, B or C) of converter m_x can be calculated as:

$$m_x = \frac{\sqrt{2} \cdot V_{Cx}}{V_{dc}/2} \quad (5)$$

where the converter output voltage V_{Cx} (phase to neutral point of three phases) can be calculated as:

$$V_{Cx} = \sqrt{\left[V_{gx}\sin(-\theta_x) + V_L\right]^2 + \left[V_{gx}\cos(-\theta_x)\right]^2} \quad (6)$$

where V_{gx} represents the voltage amplitude of bus 2 in phase X, and the voltage drop on the filter inductance V_L can be written as:

$$V_L = \omega L_f \cdot \sqrt{(I_d^+)^2 + (I_q^+)^2} \quad (7)$$

It is noted that the modulation strategy will modify the duty ratio and thereby change the shape of voltage reference for converter (phase to mid-point of DC bus). The maximum modulation index will be extended from 1 to 1.15 if some modulation strategies with zero-sequence-components are applied.

Fig. 12 shows the modulation index of the grid connected converter at various dip severity on PCC (D_1). It can be seen that the modulation index is unsymmetrical among the three phases under the unbalanced fault conditions, and the wind speeds do not have strong impacts to the modulation index of converter under various LVRT operations.

Fig. 13 indicates the power oscillation amplitude under various dip severity for the three types of grid faults, and different wind speed conditions are indicated. The oscillation amplitude of active power P_{cs2} and reactive power Q_{cs2} can be calculated as [12]:

$$P_{cs2} = \sqrt{P_{\cos2}^2 + P_{\sin2}^2} = \frac{3}{2}\sqrt{(V_d^- \cdot I_d^+)^2 + (V_d^- \cdot I_q^+)^2}$$
$$Q_{cs2} = \sqrt{Q_{\cos2}^2 + Q_{\sin2}^2} = \frac{3}{2}\sqrt{(V_d^- \cdot I_q^+)^2 + (V_d^- \cdot I_d^+)^2} \quad (8)$$

It can be seen that the oscillation amplitude P_{cs} and Q_{cs} are equal for a given grid fault condition. For the unbalanced grid faults, the two-phase fault condition introduces larger power oscillation than the one-phase grid fault during the whole range of dip severity. The maximum power oscillation amplitude under two-phase fault is 0.5 p.u. and 0.33 p.u. for one-phase fault.

It can be expected, the significant differences in the delivered power, phase angles and modulation index under various grid fault conditions may lead to significantly different loading statuses of power semiconductor devices.
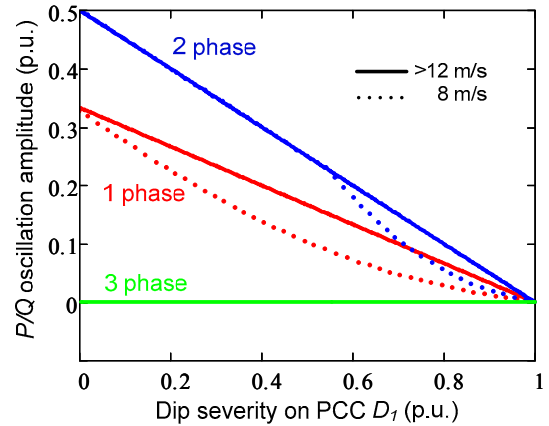

Fig. 13. Active/reactive power oscillation amplitude vs. Dip severity on PCC.
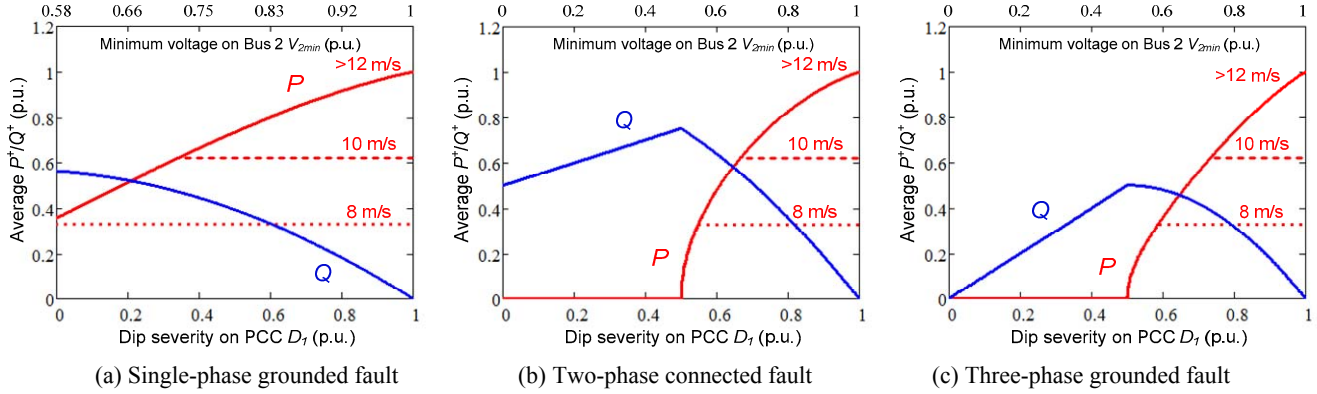
(a) Single-phase grounded fault (b) Two-phase connected fault (c) Three-phase grounded fault

Fig. 10. Active and reactive power vs. dip severity on PCC.

(a) Single-phase grounded fault (b) Two-phase connected fault (c) Three-phase grounded fault
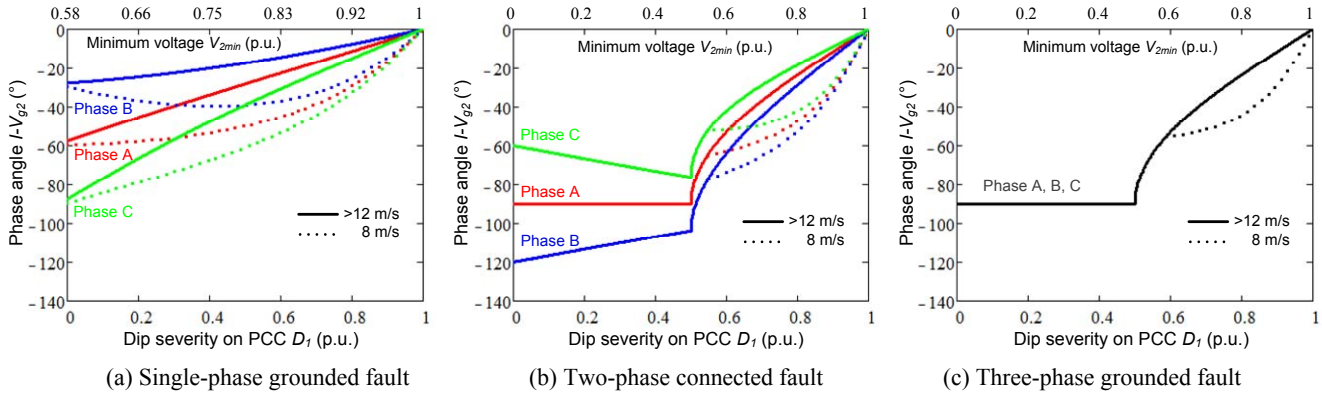
Fig. 11. Phase displacement between load current and Bus 2 voltage vs. dip severity on PCC.

(a) Single-phase grounded fault (b) Two-phase connected fault (c) Three-phase grounded fault
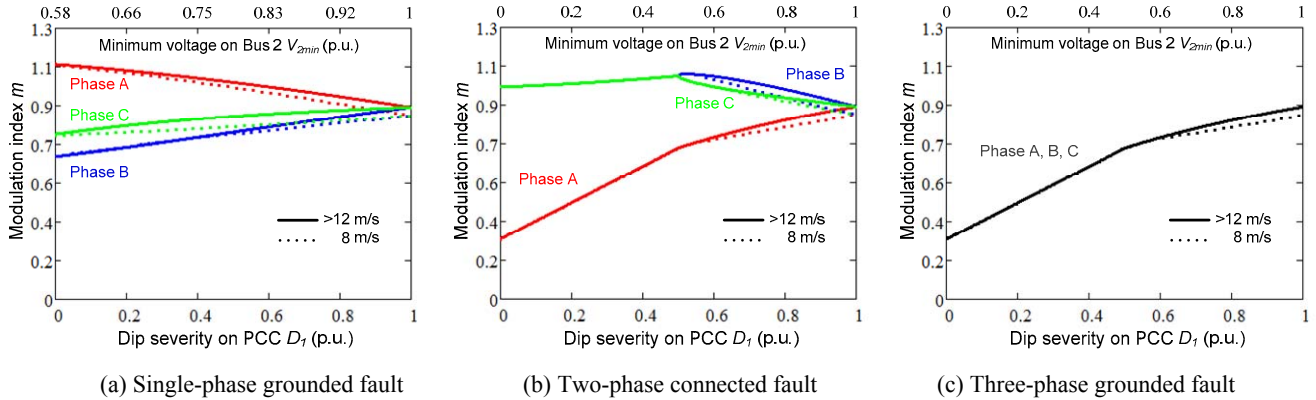
Fig. 12. Modulation index of grid converter vs. dip severity on PCC.

IV. LOSS DISTRIBUTION UNDER VARIOUS GRID FAULTS

Once the LVRT operation profiles of the grid-converter have been clarified in the previous section depending on the types and severity of voltage dips, it is possible to determine the loss distribution in the power semiconductors devices under various grid faults. The losses combined with the thermal impedance will determine the thermal behaviour of the power converter under LVRT operation, as described in the next section.

In this paper the press-pack IGCT 5SHY 40L4511 (4.5 kV/ 3.6 kA) and recommended diodes 5SDF 10H4503 are chosen as the power semiconductor devices for 3L-NPC grid connected converter [24]. The used loss model shares the same idea in [25], [26] which is a commonly accepted method for loss evaluation of power semiconductor devices, and the loss simulation is carried out based on PLECS Blockset in Simulink [26]. The average switching loss P_{sw_ave} of power devices (switches or diodes) can be calculated as:

$$P_{sw\_ave} = f_o \cdot \int_0^{1/f_o} P_{sw\_inst}(t)dt \qquad (9)$$

where the instantaneous switching loss P_{sw_inst} of power devices can be calculated by:

$$P_{sw\_inst}(t) = f_s \cdot E_{sw}\left(i_x(t),T_j\right)\cdot(V_{dc}/2V_{ref})^{K_v} \qquad (10)$$

K_v is the voltage coefficient which can be found in [27], V_{ref} is the commutated voltage tested on datasheet, f_s is the swtichign frequency. The switching energy loss of E_{sw} (E_{on}, E_{off} for switches and E_{rr} for diodes) which is function of load current $i_x(t)$ and junction temperature T_j can be expressed as:

$$E_{sw}\left(i_x(t),T_j\right) = E_{sw}\left(i_x(t)\right)\cdot\left[1+K_T\cdot(T_j-T_{ref})\right] \qquad (11)$$

where the curve for $E_{sw}(i_x(t),T_j)$ can be found in the device datasheet, K_T is the temperature coefficient which can be found in [27], T_{ref} is the reference temperature under test in the datasheet, normally at 25 ºC or 125 ºC.

Similarly the average condition loss P_{cond_ave} of power devices can be calculated as:

$$P_{cond\_ave} = f_o \cdot \int_0^{1/f_o} P_{cond\_inst}(t)dt \qquad (12)$$

where the instantaneous conduction loss P_{cond_inst} can be calculated as:

$$P_{cond\_inst}(t) = v_{cond}\left(i_x(t),T_j\right)\cdot i_x(t)\cdot D(m_x,t) \qquad (13)$$

The duty ratio $D(m_x, t)$ is a function of the modulation index m_x and related to the modulation strategy. The conduction voltage curve $v_{cond}(i_x(t),T_j)$ of power device can be found in the device datasheet, and can be analytically represented by:

$$v_{cond}\left(i_x(t),T_j\right) = \left[V_{cond0(T_{ref})}+K_{t2}\cdot(T_j-T_{ref})\right]$$
$$+i_x(t)\cdot\left[r_{cond(T_{ref})}+K_{t3}\cdot(T_j-T_{ref})\right] \qquad (14)$$

where K_{t2}, K_{t3}, $V_{cond0(Tref)}$ and $r_{cond(Tref)}$ are coefficients which can be found in [27] and the device datasheet.

It is noted that during the LVRT operation, the DC bus of the power converter may probably increase because of the short term mismatch in the input and output active power through the converter [8], [9]. The increased DC bus voltage should be limited (e.g. maximum 110 % rated) for hundreds of milliseconds by triggering the braking chopper, which normally consists of a resistor in series of a switch and is paralleled with the DC bus, as also indicated in Fig. 6. According to the loss model in [25], [26], the DC bus voltage has important impact on both of the switching loss and the conduction loss (modulation index) in power switching devices. As a result, the increased DC bus voltage should be taken into account in the loss analysis during
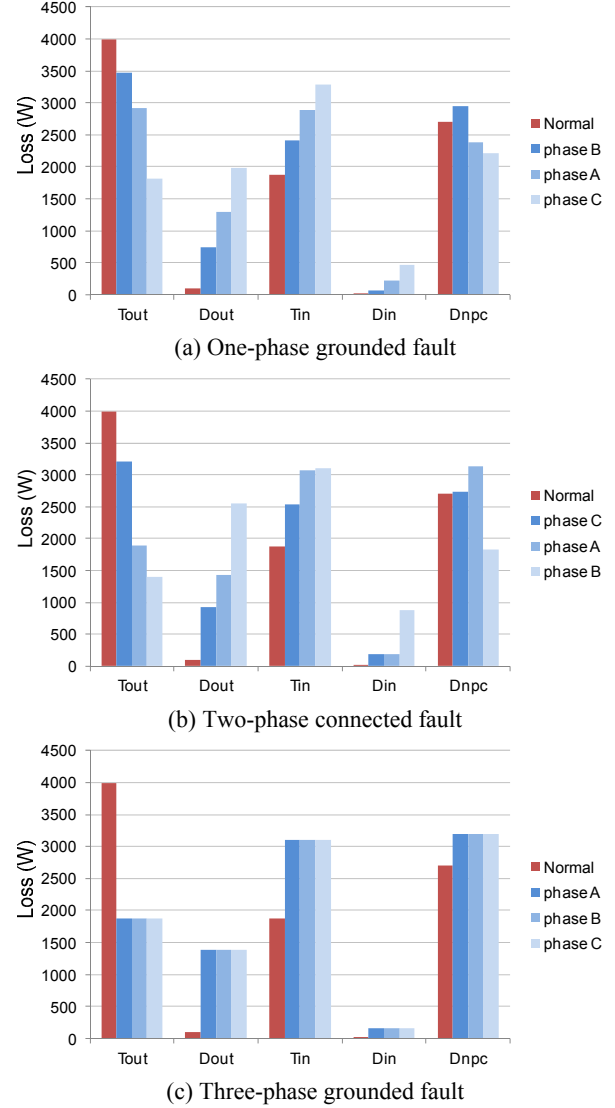

(a) One-phase grounded fault

(b) Two-phase connected fault

(c) Three-phase grounded fault

Fig. 14. Loss distribution of 3L-NPC grid converter under extreme operations (LVRT condition: v_w=12 m/s, D_I=0 p.u.. Normal condition: v_w=12 m/s, P_G=10 MW, PF=1).

LVRT operation. Moreover, the increased DC bus voltage may decrease the lifetime of power switching devices due to the cosmic radiation failure mechanism as reported in [28]. However, this issue will not be discussed in this paper.

The loss distribution of the power switching devices under the most stressed normal operation (v_w=12 m/s), and under the most stressed LVRT operation (D_I=0 p.u.), are compared in Fig. 14, where three types of grid faults are indicated in Fig. 14 (a), Fig. 14 (b) and Fig. 14 (c) respectively. The 10% higher DC bus voltage is applied for the LVRT conditions. It can be seen that, all of the three extreme LVRT operations impose the diodes and inner switches of 3L-NPC converter with significant larger losses than the normal operation condition. Moreover, the loss distribution among the three phases of converter is asymmetrical under the one-phase and two-phase unbalanced grid faults.

V. Thermal Behaviour under various Grid Faults

The thermal performance of power devices are closely related to the reliability of the converter, current rating of power devices and cost of the cooling system. Therefore it is an important indicator for full-scale wind power converters. In order to conduct thermal performance evaluation, an appropriate thermal model should first be acquired.

The thermal models for a single switch and clamping diode are indicated in Fig. 15 [24], [29], in which the thermal impedance from junction to case $Z_{(j-c)}$ is modeled as a multi-layer Foster RC network, as shown in Fig. 16. Each of the thermal parameters can be found from the manufacturer datasheets, where the thermal resistance R_{th} will decide the steady state mean value of the junction temperature, and the thermal capacitance (with time constant τ) will decide the dynamic change or fluctuation of the junction temperature.

It is noted that normally the IGCT manufacturer will only provide thermal parameters inside IGCT press-pack with Foster RC network. In order to establish the complete thermal models from junction to the ambient, the thermal impedance of $Z_{T/D(j-c)}$ has to be transferred to the equivalent
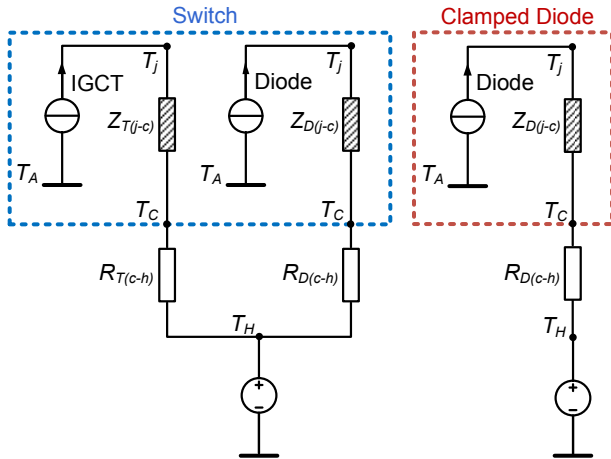
Note:

T_j: junction temperature, T_C: case temperature, T_H: heat sink temperature, T_A: ambient temperature, $Z_{(j-c)}$: thermal impedance from junction to case, $Z_{(c-h)}$: thermal impedance from case to heat sink.

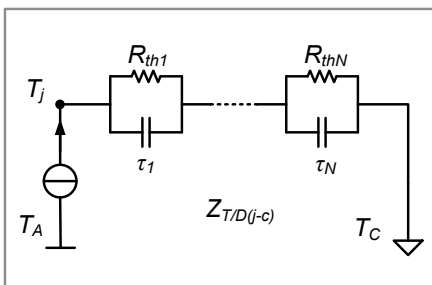Fig. 15. Thermal model of the power switching devices.

Fig. 16. Thermal model of the impedance $Z_{T(j-c)}$ or $Z_{D(j-c)}$ from junction to case.

Cauer RC network in the simulation to facilitate the thermal impedance extension [28]. Because the temperature of the heat sink T_H is normally much lower and more stable compared to the junction temperature T_j in a properly designed converter system, the heat sink temperature is considered as a constant value at 60 ℃ in this paper. However, the heat sink temperature may strongly depend on the operation site and the design of the heat sink system.

Based on the previous loss results and thermal model from datasheet, the junction temperature of the power devices under various grid faults can be investigated by the PLECS blockset in Simulink.

A. Singe-phase grounded fault

The junction temperatures for the three phases of 3L-NPC converter undergoing the extreme one-phase grounded grid fault (Type C voltage dip on Bus 2 with D_I=0 p.u., v_w=12 m/s) are shown in Fig. 17. It can be seen that the thermal loading in the three phases of the converter are slightly different from each other under this fault condition. Phase B has more stressed D_{npc} and T_{out} while phase A and phase C have more stressed T_{in}, D_{out} and D_{in}.

The mean junction temperature T_m of the switches and diodes under different dip severities of one-phase grid fault are shown in Fig. 20 (a) and Fig. 21 (a) respectively. The T_{out} and D_{npc} are the most stressed devices within the whole dipping range. It is noted that the difference of junction temperature among three phases is not so large (around 10-15 ℃ max when D_I=0 p.u.) and only becomes significant when the dip severity D_I is below 0.5 p.u. (i.e. when the converter needs to provide 100% reactive current to the power grid).
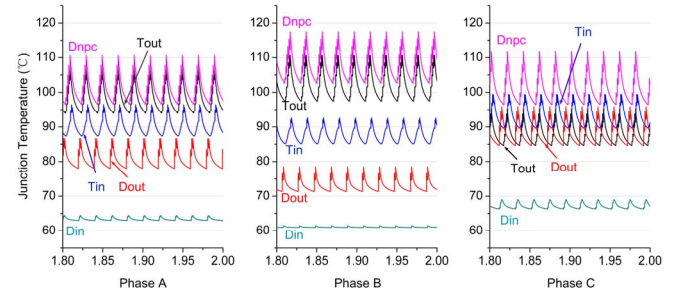

Fig. 17. Thermal distribution under one-phase grid fault (Type C voltage dip on Bus 2 with D_I=0 p.u., v_w=12 m/s, horizontal axis means time with unit of second).

B. Two-phase connected fault

The junction temperatures for the three phases of 3L-NPC converter undergoing the extreme two-phase connected grid fault (Type D voltage dip on Bus 2 with D_I=0 p.u., v_w=12 m/s) are shown in Fig. 18. It can be seen that the thermal loading behaviors in the three phases of the converter are totally different from each other.
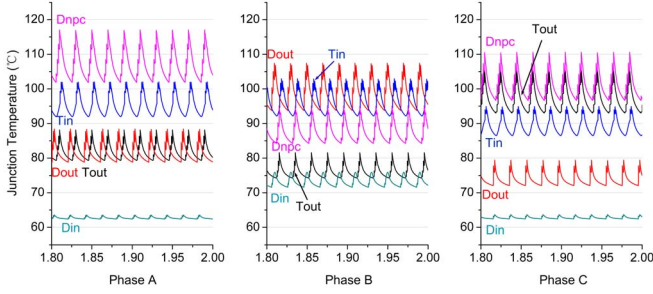
Fig. 18. Thermal distribution under two-phase grid fault (Type D voltage dip on Bus 2 with D_I=0 p.u., v_w=12 m/s, horizontal axis means time with unit of second).

The mean junction temperature T_m of the switches and diodes of two-phase grid fault are shown in Fig. 20 (b) and Fig. 21 (b) respectively. Compared to the single-phase grid

fault condition in Fig. 20 (a) and Fig. 21 (a), the junction temperature difference among the three phases of the converter is much larger (around 20-25 ℃ max when D_I=0 p.u.). Similarly, the thermal difference among three phases of converter only becomes significant when the dip severity D_I is below 0.5 p.u..

C. *Three-phase grounded fault*

The junction temperatures for the three phases of 3L-NPC converter undergoing the extreme three-phase grounded grid fault (Type A voltage dip on Bus 2 with $D_I \approx 0$ p.u., v_w=12 m/s) are shown in Fig. 19. It can be seen that the thermal loading behaviors in the three phases of the 3L-NPC converter are exactly the same under this grid fault. D_{npc} and T_{in} are the most stressed devices.
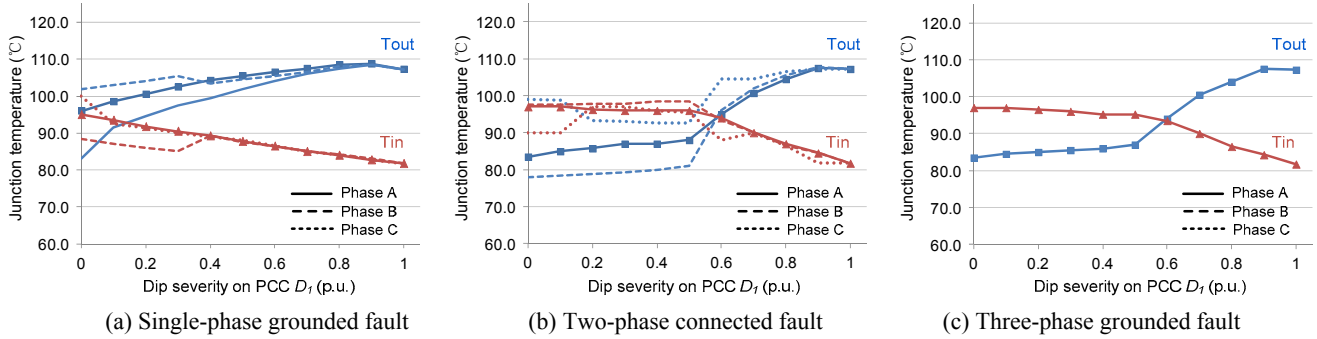

(a) Single-phase grounded fault (b) Two-phase connected fault (c) Three-phase grounded fault

Fig. 20. Junction temperature profiles of switches under various voltage dip severity (v_w=12 m/s, v_w=12 m/s, P_G=10 MW).

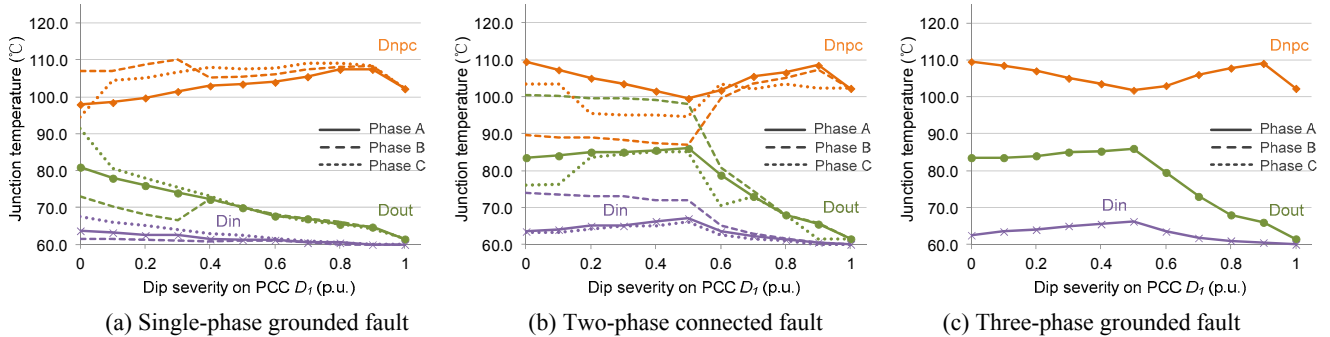(a) Single-phase grounded fault (b) Two-phase connected fault (c) Three-phase grounded fault

Fig. 21. Junction temperature profiles of diodes under various voltage dip severity (v_w=12 m/s, v_w=12 m/s, P_G=10 MW).

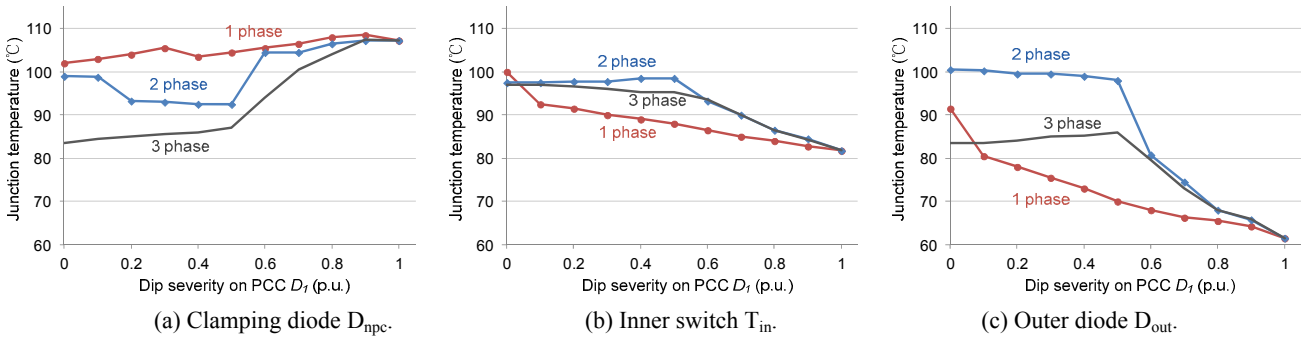(a) Clamping diode D_{npc}. (b) Inner switch T_{in}. (c) Outer diode D_{out}.

Fig. 22. Most stressed device comparison under different grid faults (v_w=12 m/s, v_w=12 m/s, P_G=10 MW).
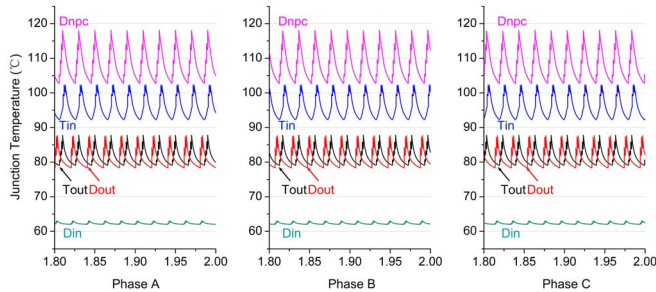
Fig. 19. Thermal distribution under three-phase grid fault (Type A voltage dip on Bus 2 with D_1=0 p.u., v_w=12 m/s, horizontal axis means time with unit of second).

The mean junction temperature T_m of the switches and the diodes under different dip severities of three-phase balance grid fault are shown in Fig. 20 (c) and Fig. 21 (c) respectively. It is interesting to see the change of junction temperature with relation to the dip severity are different when D_1 is below 0.5 p.u. and above 0.5 p.u.. This is because that there is 100% reactive current required by grid codes when D_1<0.5 p.u., this will lead to constant power factor within this range, while when D_1<0.5 p.u., there is some room for active current which will result in dramatically changed power factor.

D. Comparison

Fig. 22 presents the junction temperature comparison under different grid fault conditions, the D_{npc}, T_{in} and D_{out} in the most stressed phase of each grid fault are shown respectively. Special attention should be given to the power device T_{in}, D_{out} D_{in} and D_{npc} under the LVRT operation of 3L-NPC. In fact those devices may have even higher junction temperature than the case of the normal operation. (Up to 40℃ higher for D_{out}, 20℃ higher for T_{in}, 15℃ higher for D_{in}, and 10℃ higher for D_{npc}). This overloading should be taken into account when designing the power devices and heat sink system for the wind power converter.

VI. CONCLUSION

Because the loading conditions of power devices in the wind turbine system under grid faults are still not yet clarified, the paper aim was to investigate the impacts of various grid voltage dips on the operating and loading behaviors of full-scale wind power converter. The analyzing methods and results are important for understanding and improving the thermal behaviors of wind power converter under this adverse condition [14], [30], [31].

It has been found that the voltage dips may vary significantly on different locations (buses) in the power grid system. Depending on the types and severity of grid faults as well as LVRT control strategies, the operation status of grid connected power converter like delivered power, phase angles and modulation index are significantly different. It is interesting to notice that the operation conditions of the

power converter are unsymmetrical among the three phases when unbalanced grid faults are present.

The dramatically modified operation status under various grid faults will lead to uneven device loading not only among the three phases, but also among different types and severities of voltage dips. It should be noted that some power devices under the LVRT operation may have even higher junction temperature than the normal operation condition. This overloading should be taken into account when designing the power devices and heat sink system for the wind power converter.

REFERENCES

[1] REN21-Renewables 2012 Global Status Report, June, 2012. (Available: http://www.ren21.net).

[2] F. Blaabjerg, Z. Chen, S.B. Kjaer, "Power Electronics as Efficient Interface in Dispersed Power Generation Systems", *IEEE Trans. on Power Electronics*, 2004, vol. 19, no. 4, pp. 1184-1194.

[3] Z. Chen, J.M. Guerrero, F. Blaabjerg, "A Review of the State of the Art of Power Electronics for Wind Turbines," *IEEE Trans. on Power Electronics*, vol.24, no.8, pp.1859-1875, Aug. 2009.

[4] Website of Vestas Wind Power, *Wind turbines overview*, April 2011. (Available: http://www.vestas.com/)

[5] M. Altin, O. Goksu, R. Teodorescu, P. Rodriguez, B. Bak-Jensen, L. Helle, "Overview of recent grid codes for wind power integration," *Proc. of OPTIM' 2010*, pp.1152-1160, 2010.

[6] E.ON-Netz – Grid Code. High and extra high voltage, April 2006.

[7] F. Blaabjerg, M. Liserre, K. Ma, "Power Electronics Converters for Wind Turbine Systems," *IEEE Trans. on Industry Applications*, vol. 48, no. 2, pp. 708-719, 2012.

[8] S.M.Muyeen, R.Takahashi, T.Murata, J.Tamura, "A Variable Speed Wind Turbine Control Strategy to Meet Wind Farm Grid Code Requirements," *IEEE Trans. on Power Systems*, 2010, vol. 25, no. 1, pp. 331-340.

[9] S. Alepuz, S. Busquets-Monge, J. Bordonau, J.A. Martinez-Velasco, C.A. Silva, J. Pontt, J. Rodriguez, "Control Strategies Based on Symmetrical Components for Grid-Connected Converters Under Voltage Dips," *IEEE Trans. on Industrial Electronics*, vol. 56, no. 6, pp. 2162-2173, 2009.

[10] P. Rodríguez, A. Luna, R. Muñoz-Aguilar, I. Etxeberria-Otadui, R. Teodorescu, F. Blaabjerg, "A Stationary Reference Frame Grid Synchronization System for Three-Phase Grid-Connected Power Converters Under Adverse Grid Conditions," *IEEE Trans. on Power Electronics*, Vol. 27, No. 1, pp. 99-112, Jan 2012.

[11] P. Rodriguez, A.V. Timbus, R. Teodorescu, M. Liserre, F. Blaabjerg, "Flexible Active Power Control of Distributed Power Generation Systems During Grid Faults," *IEEE Trans. on Industrial Electronics*, vol. 54, no. 5, pp. 2583-2592, 2007.

[12] Hong-Seok Song, Kwanghee Nam, "Dual current control scheme for PWM converter under unbalanced input voltage conditions," *IEEE Trans. on Industrial Electronics*, vol. 46, no. 5, pp. 953-959, 1999.

[13] K. Ma, F. Blaabjerg, M. Liserre, "Thermal Analysis of Multilevel Grid Side Converters for 10 MW Wind Turbines under Low Voltage Ride Through," *IEEE Trans. on Industry Applications, 2013.*

[14] K. Ma, F. Blaabjerg, "Thermal Optimized Modulation Method of Three-level NPC Inverter for 10 MW Wind Turbines under Low Voltage Ride Through," *IET Journal on Power Electronics*, vol. 5, no. 6, pp. 920-927, 2012.

[15] G. Saccomando, J. Svensson, A. Sannino, "Improving voltage disturbance rejection for variable-speed wind turbines," *IEEE Trans. on Energy Conversion*, vol. 17, no. 3, pp. 422-428, 2002.

[16] R. Teodorescu, M. Liserre, P. Rodriguez, *Grid Converters for Photovoltaic and Wind Power Systems*, Wiley-IEEE press, 2011

[17] S. Kouro, M. Malinowski, K. Gopakumar, J. Pou, L. G. Franquelo, B. Wu, J. Rodriguez, M. A. Perez, J. I. Leon, "Recent Advances and Industrial Applications of Multilevel Converters," *IEEE Trans. on Power Electronics*, vol. 57, no. 8, pp. 2553–2580, 2010.

[18] O. S. Senturk, L. Helle, S. Munk-Nielsen, P. Rodriguez, R. Teodorescu, "Medium voltage three-level converters for the grid connection of a multi-MW wind turbine," in *Proc. of EPE'2009*, pp: 1- 8, 2009.

[19] K. Ma, F. Blaabjerg, D. Xu, "Power Devices Loading in Multilevel Converters for 10 MW Wind Turbines," in *Proc. of ISIE' 2011*, pp. 340-346, June 2011.

[20] K. Ma, F. Blaabjerg, "Multilevel Converters for 10 MW Wind Turbines," in *Proc. of EPE' 2011*, August 2011.

[21] H. Li, Z. Chen, H. Polinder, "Optimization of Multibrid Permanent-Magnet Wind Generator Systems," *IEEE Trans. on Energy Conversion,* vol. 24, no. 1, pp. 82-92, 2009.

[22] H.Polinder, F.F.A.van der Pijl, G.-J.de Vilder, P.J.Tavner, "Comparison of direct-drive and geared generator concepts for wind turbines," *IEEE Trans. on Energy Conversion,* vol. 21, no. 3, pp. 725-733, 2006.

[23] K. Ma, M. Liserre, F. Blaabjerg, "Reactive power control methods for improved reliability of wind power inverters under wind speed variations," in *Proc. of ECCE'2012*, pp: 3105- 3112, 2012.

[24] ABB Application Note: Applying IGCTs, May 2007.

[25] F. Blaabjerg, U. Jaeger, S. Munk-Nielsen and J. Pedersen, "Power Losses in PWM-VSI Inverter Using NPT or PT IGBT Devices," *IEEE Trans. on Power Electronics,* vol. 10, no. 3, pp. 358–367, May 1995.

[26] Semikron Application Note: *3L NPC & TNPC Topology*, AN-11001, 2011.

[27] A. Wintrich, U. Nicolai, W. Tursky, T. Reimann, *Application Manual power Semiconductors*, Seimikron International GmbH, Nov. 2010.

[28] N. Kaminski, A. Kopta, "Failure rates of HiPak Modules due to cosmic rays," ABB application note 5SYA 2042-04, Mar 2011.

[29] User manual of PLECS blockset version 3.1, March 2011. (Available: http://www.plexim.com/files/plecsmanual.pdf).

[30] K. Ma, F. Blaabjerg, "Loss and thermal redistributed modulation methods for three-level neutral-point-clamped wind power inverter undergoing Low Voltage Ride Through", *Proc. of ISIE' 2012*, pp. 1880-1887, 2012.

[31] K. Ma, F. Blaabjerg, M. Liserre, "Power Controllability of Three-phase Converter with Unbalance AC Source," *Proc. of APEC' 2013*, 2013.